Inorganic Chemistry
Article

Inorg. Chem. **2010**, *49*, 6883–6888 **6883**
DOI: 10.1021/ic100266n

Phosphate Mono- and Diesterase Activities of the Trinuclear Zinc Enzyme Nuclease P1—Insights from Quantum Chemical Calculations

Rong-Zhen Liao,[†,‡] Jian-Guo Yu,[‡] and Fahmi Himo*[,†]

[†]*Department of Organic Chemistry, Arrhenius Laboratory, Stockholm University, SE-10691 Stockholm, Sweden, and* [‡]*College of Chemistry, Beijing Normal University, Beijing, 100875, People's Republic of China*

Received February 9, 2010

Nuclease P1 is a trinuclear zinc enzyme that catalyzes the hydrolysis of single-stranded DNA and RNA. Density functional calculations are used to elucidate the reaction mechanism of this enzyme with a model of the active site designed on the basis of the X-ray crystal structure. 2-Tetrahydrofuranyl phosphate and methyl 2-tetrahydrofuranyl phosphate substrates are used to explore the phosphomonoesterase and phosphodiesterase activities of this enzyme, respectively. The calculations reveal that for both activities, a bridging hydroxide performs an in-line attack on the phosphorus center, resulting in inversion of the configuration. Simultaneously, the P−O bond is cleaved, and Zn2 stabilizes the negative charge of the leaving alkoxide anion and assists its departure. All three zinc ions, together with Arg48, provide electrostatic stabilization to the penta-coordinated transition state, thereby lowering the reaction barrier.

I. Introduction

Recognition of nucleic acids by proteins is of fundamental importance in biology, especially in the regulation of genetic expression.[1] Nuclease P1 from *Penicillium citrinum* is a member of the zinc-dependent extracellular endonuclease family and exhibits high cleavage specificity for single-stranded DNA, RNA, or double-stranded DNA with mismatches, but not natural double-stranded DNA.[2] It functions as a phosphodiesterase to cleave the P−$O_{3'}$ bond with inversion of the configuration at the phosphorus center (Scheme 1).[3] It can also function as a phosphomonoesterase, removing the 3′-terminal phosphate group.[2a,b]

The X-ray crystal structure of nuclease P1 has been solved, and it revealed that this enzyme has almost identical disposition and coordination of the three zinc ions in the active site as phospholipase C from *Bacillus cereus* (PLC_{BC}).[4] Zn1 is coordinated by two histidines (His60 and His116) and an aspartate (Asp45); Zn2 is bound to two other histidines (His149 and His126) and an aspartate (Asp153); while Zn3 is ligated by a histidine (His6) and a tryptophan (Trp1). Zn1 and Zn3 are bridged by an aspartate (Asp120).[4d] It is believed that these two zinc ions are also bridged by a hydroxide ion.[4d] This suggestion is based on the similarity with the PLC_{BC} active site. A second-shell residue, Arg48, is proposed to interact with the phosphate substrate.[4d] In PLC_{BC}, there is no such arginine residue in the active site, although the two enzymes catalyze a similar kind of reaction. The structure of the native enzyme in complex with a product analogue, dithiophosphorylated oligonucleotide d[A(pS2)T(pS2)T-(pS2)T] (called ATTT in short), is shown in Figure 1. The terminal $O_{3'}$ hydroxyl of ATTT coordinates to Zn2, replacing a water ligand. It has been suggested that this binding model represents the binding of the natural substrate, as the dithiophosphotate group, lying outside the active site pocket, has little influence on the phosphate binding.[4d]

On the basis of the structural studies and also other biochemical experiments,[3] the following reaction mechanism has been proposed for nuclease P1 (Scheme 2).[4d] The substrate first docks into the active site with its phosphate O_R bridging Zn2 and Zn3 and O_S coordinating to Zn1. Arg48 also helps in substrate binding and orientation through hydrogen bonds to the phosphate O_S and $O_{5'}$ oxygens. The hydroxide bridging Zn1 and Zn3 then acts as a nucleophile making an in-line attack on the phosphorus center. Asp45 is

*To whom correspondence should be addressed. E-mail: himo@organ.su.se.

(1) (a) Jones, S.; van Heyningen, P.; Berman, H. M.; Thornton, J. M. *J. Mol. Biol.* **1999**, *287*, 877–896. (b) Jones, S.; Daley, D. T.; Luscombe, N. M.; Berman, H. M.; Thornton, J. M. *Nucleic Acids Res.* **2001**, *29*, 943–954. (c) Luscombe, N. M.; Laskowski, R. A.; Thornton, J. M. *Nucleic Acids Res.* **2001**, *29*, 2860–2874. (d) Hoffman, M. M.; Khrapov, M. A.; Cox, J. C.; Yao, J.; Tong, L.; Ellington, A. D. *Nucleic Acids Res.* **2004**, *32*, D174–D181.

(2) (a) Fujimoto, M.; Kuninaka, A.; Yoshino, H. *Agr. Biol. Chem.* **1974**, *38*, 785–790. (b) Fujimoto, M.; Kuninaka, A.; Yoshino, H. *Agr. Biol. Chem.* **1974**, *38*, 1555–1561. (c) Fujimoto, M.; Fujiyama, K.; Kuninaka, A.; Yoshino, H. *Agr. Biol. Chem.* **1974**, *38*, 2141–2147. (d) Fujimoto, M.; Kuninaka, A.; Yoshino, H. *Agr. Biol. Chem.* **1975**, *39*, 1991–1997. (e) Naik, A. K.; Raghavan, S. C. *DNA Repair* **2008**, *7*, 1384–1391.

(3) Potter, B. V. L.; Connolly, B. A.; Eckstein, F. *Biochemistry* **1983**, *22*, 1369–1377.

(4) (a) Lahm, A.; Volbeda, A.; Suck, D. *J. Mol. Biol.* **1990**, *215*, 207–210. (b) Volbeda, A.; Lahm, A.; Sakiyama, F.; Suck, D. *EMBO J.* **1991**, *10*, 1607–1618. (c) Maekawa, K.; Tsunasawa, S.; Dibó, G.; Sakiyama, F. *Eur. J. Biochem.* **1991**, *200*, 651–661. (d) Romier, C.; Dominguez, R.; Lahm, A.; Dahl, O.; Suck, D. *Proteins* **1998**, *32*, 414–424. (e) Hough, E.; Hansen, L. K.; Birknes, B.; Jynge, K.; Hansen, S.; Hordvik, A.; Little, C.; Dodson, E.; Derewenda, Z. *Nature* **1989**, *338*, 357–360. (f) Benfield, A. P.; Goodey, N. M.; Phillips, L. T.; Martin, S. F. *Arch. Biochem. Biophys.* **2007**, *460*, 41–47.

© 2010 American Chemical Society
Published on Web 07/06/2010

Scheme 1. Reaction Catalyzed by Nuclease P1

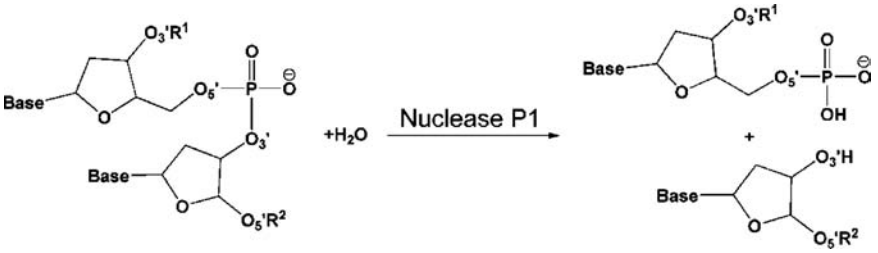

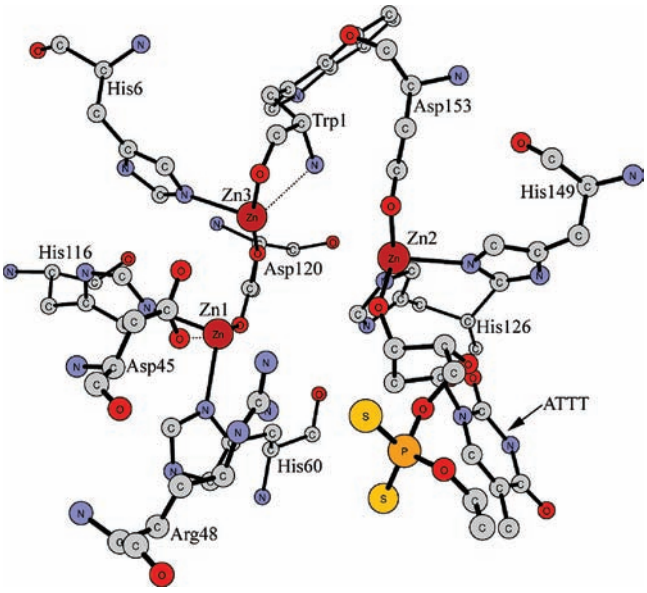

Figure 1. X-ray crystal structure of active site of nuclease P1 in complex with dithiophosphorylated oligonucleotide d[A(pS2)T(pS2)T(pS2)T]. Coordinates taken from PDB entry 1AK0.[4d]

believed to help in orienting the hydroxide for the nucleophilic attack, and Zn2 plays a crucial role in stabilizing the leaving $O_{3'}$ oxyanion. Such an in-line attack results in inversion of the configuration at the phosphorus center, consistent with NMR data.[3] This reaction mechanism is almost identical to that of another trinuclear zinc enzyme, namely, endonuclease IV, which catalyzes the hydrolytic cleavage of the P−$O_{3'}$ bond at the 5′ position of abasic sites.[5]

In the present study, density functional theory (DFT) has been employed to investigate the reaction mechanism of phosphate hydrolysis utilized by nuclease P1. A model of the active site is devised from the crystal structure (PDB code 1AK0).[4d] The hybrid functional B3LYP[6] is used to calculate the potential energy profiles for the hydrolysis of both phosphate monoester and diester substrates. The quantum chemical cluster methodology has been successfully applied to study a wide variety of enzymes,[7] including several related zinc enzymes.[8] Most relevantly, very recent calculations on the above-mentioned trinuclear zinc enzyme PLC_{BC} showed that the adopted protocol performs quite well in elucidating the reaction mechanism of phosphate hydrolysis.[8h] Furthermore, that study established that, for PLC_{BC}, the bridging hydroxide performs a nucleophilic attack on the phosphate, with a concomitant departure of the leaving alkoxide, which takes a proton from a water molecule bound to the third zinc ion.[8h]

II. Computational Details

All calculations were performed using the density functional theory (DFT) functional B3LYP,[7] as implemented in the Gaussian03 program package.[9] Benchmark tests of several density functionals in the determination of geometrical properties of biological zinc complexes showed that B3LYP had a quite good performance.[10] In general, the error in B3LYP has been estimated to be 3−5 kcal/mol for enzyme modeling involving transition metals.[11]

Geometry optimizations were carried out with the 6-311+G(2d) basis set for P and the five oxygen atoms around it (the attacking oxygen, the leaving oxygen, and the other three directly coordinated oxygens), the LANL2DZ[12] basis set for Zn, and the 6-31G(d,p) basis set for all other atoms. On the basis of these optimized geometries, the energies were evaluated by performing single-point calculations using the 6-311+G(2d,2p) basis set for all elements.

(5) Ivanov, I.; Tainer, J. A.; MaCammon, J. A. *Proc. Natl. Acad. Sci. U.S.A.* **2007**, *104*, 1465–1470.
(6) (a) Becke, A. D. *J. Chem. Phys.* **1993**, *98*, 5648–5652. (b) Lee, C.; Yang, W.; Parr, R. G. *Phys. Rev. B* **1988**, *37*, 785–789.
(7) (a) Blomberg, M. R. A.; Siegbahn, P. E. M. *J. Phys. Chem. B* **2001**, *105*, 9375–9386. (b) Himo, F.; Siegbahn, P. E. M. *Chem. Rev.* **2003**, *103*, 2421–2456. (c) Noodleman, L.; Lovell, T.; Han, W.-G.; Li, J.; Himo, F. *Chem. Rev.* **2004**, *104*, 459–508. (d) Siegbahn, P. E. M.; Borowski, T. *Acc. Chem. Res.* **2006**, *39*, 729–738. (e) Himo, F. *Theor. Chem. Acc.* **2006**, *116*, 232–240. (f) Ramos, M. J.; Fernandes, P. A. *Acc. Chem. Res.* **2008**, *41*, 689–698. (g) Himo, F.; Siegbahn, P. E. M. *J. Biol. Inorg. Chem.* **2009**, *14*, 643–651. (h) Blomberg, M. R. A.; Siegbahn, P. E. M. *Biochim. Biophys. Acta* **2010**, *1797*, 129–142.
(8) (a) Chen, S.-L.; Fang, W.-H.; Himo, F. *J. Phys. Chem. B* **2007**, *111*, 1253–1255. (b) Chen, S.-L.; Marino, T.; Fang, W.-H.; Russo, N.; Himo, F. *J. Phys. Chem. B* **2008**, *112*, 2494–2500. (c) Liao, R.-Z.; Yu, J.-G.; Raushel, F. M.; Himo, F. *Chem.—Eur. J.* **2008**, *14*, 4287–4292. (d) Liao, R.-Z.; Yu, J.-G.; Himo, F. *Inorg. Chem.* **2009**, *48*, 1442–1448. (e) Chen, S.-L.; Fang, W.-H.; Himo, F. *J. Inorg. Biochem.* **2009**, *103*, 274–281. (f) Liao, R.-Z.; Himo, F.; Yu, J.-G.; Liu, R.-Z. *Eur. J. Inorg. Chem.* **2009**, *20*, 2967–2972. (g) Liao, R.-Z.; Himo, F.; Yu, J.-G.; Liu, R.-Z. *J. Inorg. Biochem.* **2010**, *104*, 37–46. (h) Liao, R.-Z.; Yu, J.-G.; Himo, F. *J. Phys. Chem. B.* **2010**, *114*, 2533–2540.
(9) Frisch, M. J.; Trucks, G. W.; Schlegel, H. B.; Scuseria, G. E.; Robb, M. A.; Cheeseman, J. R.; Montgomery, J. A., Jr.; Vreven, T.; Kudin, K. N.; Burant, J. C.; Millam, J. M.; Iyengar, S. S.; Tomasi, J.; Barone, V.; Mennucci, B.; Cossi, M.; Scalmani, G.; Rega, N.; Petersson, G. A.; Nakatsuji, H.; Hada, M.; Ehara, M.; Toyota, K.; Fukuda, R.; Hasegawa, J.; Ishida, M.; Nakajima, T.; Honda, Y.; Kitao, O.; Nakai, H.; Klene, M.; Li, X.; Knox, J. E.; Hratchian, H. P.; Cross, J. B.; Bakken, V.; Adamo, C.; Jaramillo, J.; Gomperts, R.; Stratmann, R. E.; Yazyev, O.; Austin, A. J.; Cammi, R.; Pomelli, C.; Ochterski, J. W.; Ayala, P. Y.; Morokuma, K.; Voth, G. A.; Salvador, P.; Dannenberg, J. J.; Zakrzewski, V. G.; Dapprich, S.; Daniels, A. D.; Strain, M. C.; Farkas, O.; Malick, D. K.; Rabuck, A. D.; Raghavachari, K.; Foresman, J. B.; Ortiz, J. V.; Cui, Q.; Baboul, A. G.; Clifford, S.; Cioslowski, J.; Stefanov, B. B.; Liu, G.; Liashenko, A.; Piskorz, P.; Komaromi, I.; Martin, R. L.; Fox, D. J.; Keith, T.; Al-Laham, M. A.; Peng, C. Y.; Nanayakkara, A.; Challacombe, M.; Gill, P. M. W.; Johnson, B.; Chen, W.; Wong, M. W.; Gonzalez, C.; Pople, J. A. *Gaussian 03*, Revision D.01; Gaussian, Inc.: Wallingford, CT, 2004.
(10) (a) Sousa, S. F.; Fernandes, P. A.; Ramos, M. J. *J. Phys. Chem. B* **2007**, *111*, 9146–9152. (b) Sousa, S. F.; Carvalho, E. S.; Ferreira, D. M.; Tavares, I. S.; Fernandes, P. A.; Ramos, M. J.; Gomes, J. A. N. F. *J. Comput. Chem.* **2009**, *30*, 2752–2763. (c) Sorkin, A.; Truhlar, D. G.; Amin, E. A. *J. Chem. Theory Comput.* **2009**, *5*, 1254–1265.
(11) Siegbahn, P. E. M. *J. Biol. Inorg. Chem.* **2006**, *11*, 695–701.
(12) Hay, P. J.; Wadt, W. R. *J. Chem. Phys.* **1985**, *82*, 270–283.

Scheme 2. Proposed Substrate Binding and Reaction Mechanism of Nuclease P1[4d]

To evaluate the sensitivity of the results to the choice of functional, we have performed single-point calculations (with the large basis set) for the hydrolysis of the phosphomonoester substrate using the B3LYP* (with 15% exact exchange),[13] B3PW91,[14] and MPWB1K[15] methods based on the B3LYP-optimized geometries. The calculated barriers are 10.8, 10.3, and 12.8 kcal/mol using B3LYP*, B3PW91, and MPWB1K, respectively. The values are very close to the B3LYP barrier of 12.0 kcal/mol, further confirming the adequacy of the B3LYP method for these kinds of applications.

We have also examined the sensitivity of the geometries and energies to the choice of the LANL2DZ basis set used for the zinc ions. As an alternative, we used the SDD basis set[16] and reoptimized the geometries for the hydrolysis of the phosphomonoester substrate. We found that the geometries are very close to those obtained with LANL2DZ basis sets. For example, the Zn1−Zn3 distance in $React_{Mono}$ is 3.44 and 3.50 Å with LANL2DZ and SDD basis sets, respectively. Also, at TS_{Mono}, the critical O_A−P and P−O_L distances with SDD are 1.92 and 2.17 Å, respectively, compared to 1.86 and 2.27 Å with LANL2DZ. More importantly, the differences of the relative energies with the larger basis sets 6-311+G(2d,2p) based on geometries optimized with these two different basis sets are less than 2 kcal/mol. For example, the barrier is 11.4 kcal/mol at the B3LYP/6-311+G(2d,2p)//LANL2DZ level, while it is 12.9 kcal/mol with B3LYP/6-311+G(2d,2p)//SDD.

Wiberg bond indices (WBI)[17] were computed on the optimized structures at the same level of theory as the geometry optimizations using NBO5.G embedded in the Gaussian03 program.[18]

Vibrational frequency calculations were performed at the same theory level as the geometry optimization to obtain zero-point energies (ZPE) and to confirm the nature of various stationary points. As will be discussed below, a number of atoms were kept fixed to their X-ray crystal structure positions during the geometry optimizations. This leads to a few small imaginary frequencies, typically on the order of 10*i* to 30*i* cm^{-1}. These frequencies do not contribute significantly to the ZPE and can be ignored.

To estimate the effects of the protein environment, solvation effects were calculated at the same theory level as the optimizations by performing single-point calculations on the optimized structures using the CPCM method.[19] The dielectric constant ε was chosen to be 4, which is a value commonly used in modeling protein surroundings. The energies below are reported with and without this correction.

To test whether the particular choice of the continuum method can influence the results, we recalculated again the case hydrolysis of the phosphomonoester substrate using the IEF-PCM method.[20] The difference was less than 0.4 kcal/mol, indicating that the results are not sensitive to the choice of solvation model.

III. Active Site Model

The quantum chemical model of the nuclease P1 active site is constructed on the basis of the crystal structure of the enzyme in complex with dithiophosphorylated oligonucleotide (PDB code: 1AK0).[4d] The model consists of the three zinc ions along with their first-shell ligands: Trp1, His6, Asp45, His60, His116, His126, His149, and Asp153. The proposed hydroxide nucleophile was added to bridge Zn1 and Zn3. In addition, Arg48, an important second shell residue, is also included in the model. Hydrogen atoms were added manually, and the amino acids were truncated such that histidines were represented by methylimidazoles, aspartates by acetates, arginine by methyl-guanidine, and the terminal part of Trp1 by aminoacetaldehyde. To avoid large artificial movements of the various active site groups and to keep the optimized structures close to the experimental one, the truncation atoms were kept fixed to their positions from the X-ray structure. The fixed atoms are marked with asterisks in the figures below.

To study the phosphomonoesterase and phosphodiesterase activities of this enzyme, two model substrates were considered here. In the first case, a 2-tetrahydrofuranyl phosphate was added to coordinate to the three zinc ions and form a hydrogen bond to Arg48 (see $React_{Mono}$), and in the second case, a methyl 2-tetrahydrofuranyl phosphate was used instead. The substrates were placed manually in the active site to bind according to the suggestion of Romier et al., based on crystal structural analysis and NMR data.[3,4d] The total size of the models is 125 and 129 atoms, respectively, and the total charge is +1 and +2, respectively.

IV. Results and Discussion

In this study, we consider the hydrolysis of both phosphate monoester and diester substrates. The Michaelis complexes of the active site of nuclease P1 and each of the substrates (labeled $React_{Mono}$ and $React_{Di}$, respectively) were optimized and are displayed in Figures 2 and 3, respectively. Since the phosphate monoester substrate in $React_{Mono}$ has one more negative charge, the distances between the zinc ions and the phosphate oxygens are slightly shorter than those in $React_{Di}$, implying a more compact structure in $React_{Mono}$. The Zn1−Zn2, Zn1−Zn3, and Zn2−Zn3 distances in $React_{Mono}$ are 5.67, 3.44, and 4.12 Å, respectively, while the corresponding ones in $React_{Di}$ are 5.85, 3.50, and 4.39 Å, respectively. Both of these sets of values are in reasonable agreement with

(13) (a) Salomon, O.; Reiher, M.; Hess, B. A. *J. Chem. Phys.* **2002**, *117*, 4729–4737. (b) Reiher, M.; Salomon, O.; Hess, B. A. *Theor. Chem. Acc.* **2001**, *107*, 48–55.
(14) Perdew, J. P.; Wang, Y. *Phys. Rev. B* **1992**, *45*, 13244–13249.
(15) Zhao, Y.; Truhlar, D. G. *J. Phys. Chem. A* **2004**, *108*, 6908–6918.
(16) Dolg, M.; Wedig, U.; Stoll, H.; Preuss, H. *J. Chem. Phys.* **1987**, *86*, 866–872.
(17) Wiberg, K. B. *Tetrahedron* **1968**, *24*, 1083–1096.
(18) Glendening, E. D.; Badenhoop, J. K.; Reed, A. E.; Carpenter, J. E.; Bohmann, J. A.; Morales, C. M.; Weinhold, F. *NBO, 5.G*; University of Wisconsin: Madison, WI, 2001.
(19) (a) Klamt, A.; Schüürmann, G. *J. Chem. Soc., Perkin. Trans.* **1993**, *2*, 799–805. (b) Andzelm, J.; Kölmel, C.; Klamt, A. *J. Chem. Phys.* **1995**, *103*, 9312–9320. (c) Barone, V.; Cossi, M. *J. Phys. Chem. A* **1998**, *102*, 1995–2001. (d) Cossi, M.; Gega, N.; Scalmani, G.; Barone, V. *J. Comput. Chem.* **2003**, *24*, 669–691.
(20) (a) Cancès, E.; Mennucci, B.; Tomasi, J. *J. Chem. Phys.* **1997**, *107*, 3032–3041. (b) Mennucci, B.; Tomasi, J. *J. Chem. Phys.* **1997**, *106*, 5151–5158. (c) Cossi, M.; Scalmani, G.; Rega, N.; Barone, V. *J. Chem. Phys.* **2002**, *117*, 43–54.

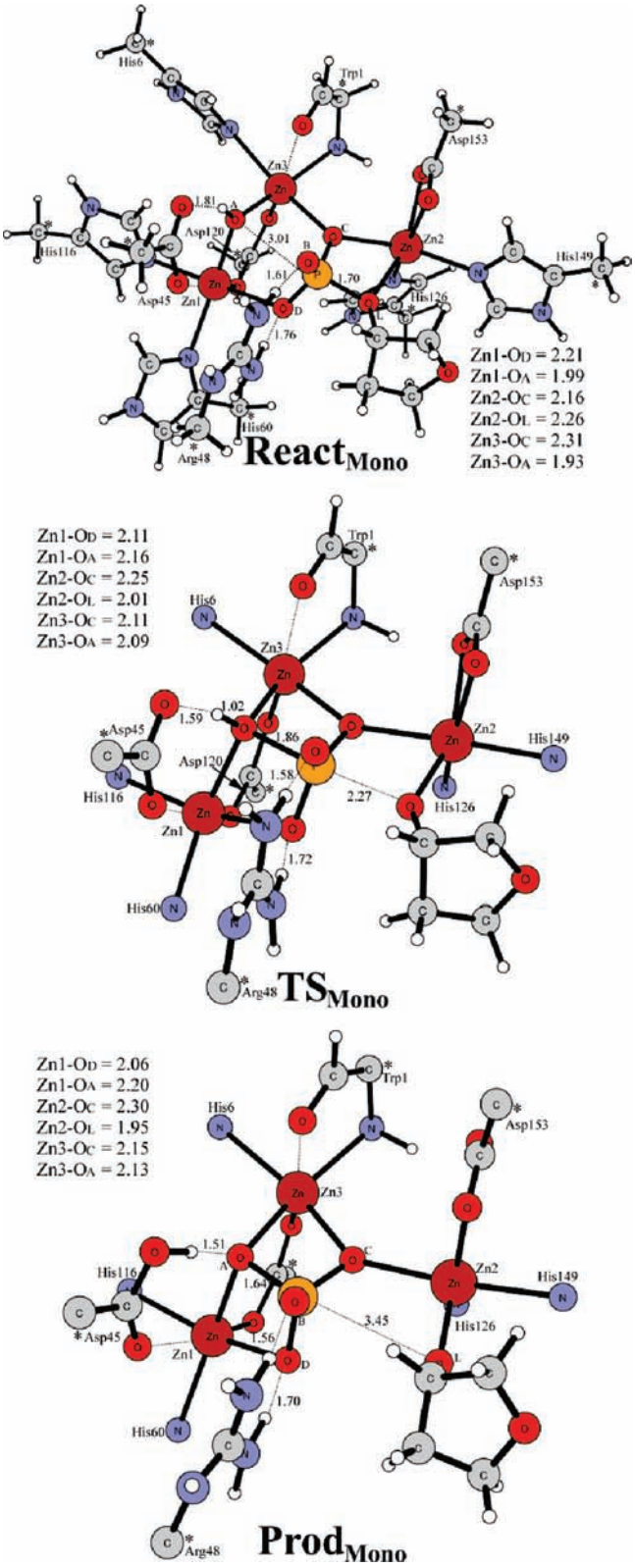

Figure 2. Optimized structures of the reactant, transition state, and product for phosphomonoester hydrolysis. Atoms marked with asterisks were fixed at their X-ray structure positions. Distances are given in Ångstroms. For clarity, the full model is given only for the reactant structure $React_{Mono}$. For TS_{Mono} and $Prod_{Mono}$, the imidazoles are represented by a nitrogen atom and some hydrogen atoms omitted.

the ones found in the crystal structure (5.86 Å, 3.67 Å, and 4.62 Å), which has a product analogue bound to Zn2.[4d]

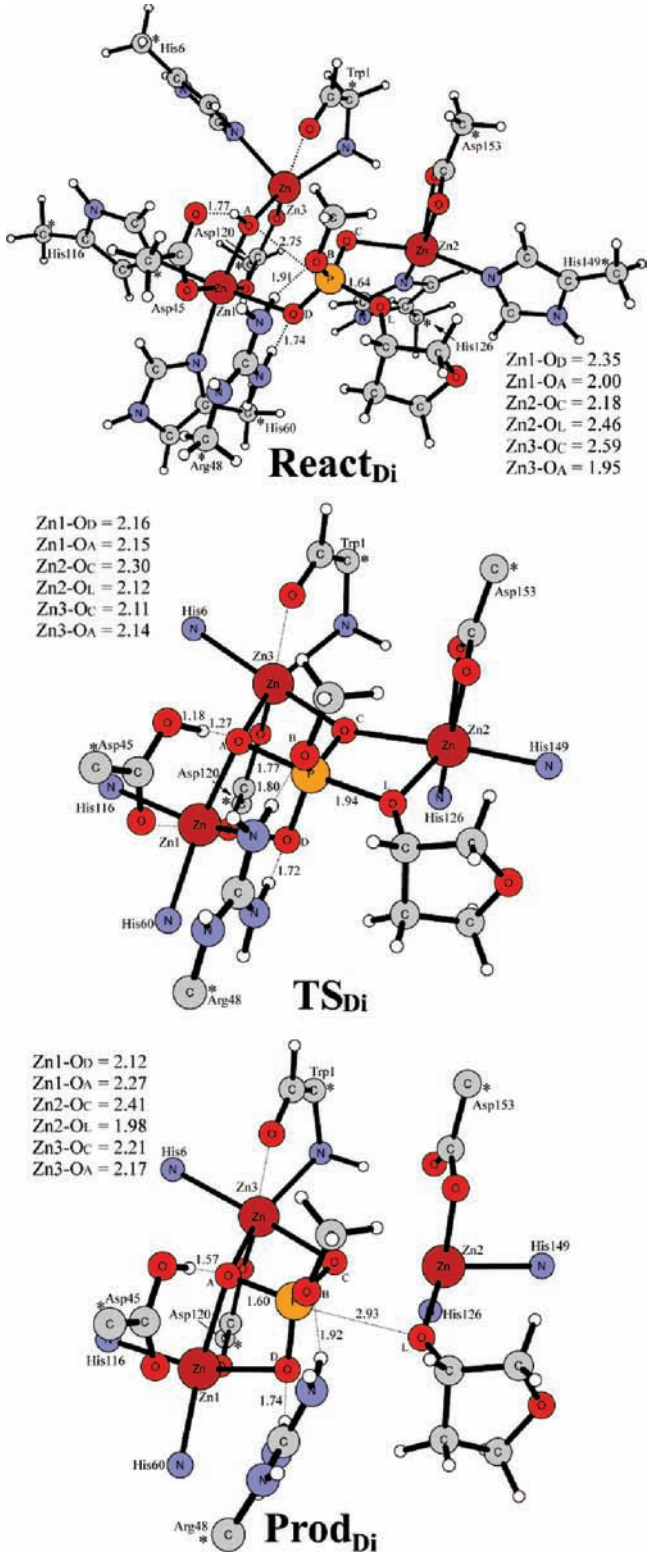

Figure 3. Optimized structures of the reactant, transition state, and product for phosphodiester hydrolysis.

Binding of the substrate makes the improper phosphate dihedral angle of $O_B-P-O_C-O_D$ larger, as it is approximately $-120°$ in solution, while it becomes $-139°$ in $React_{Mono}$ and $-131°$ in $React_{Di}$. This indicates a more open conformation after binding, which could facilitate the nucleophilic attack. In addition, the hydroxide bridging Zn1 and Zn3 is well-arranged for an in-line attack on the phosphorus center.

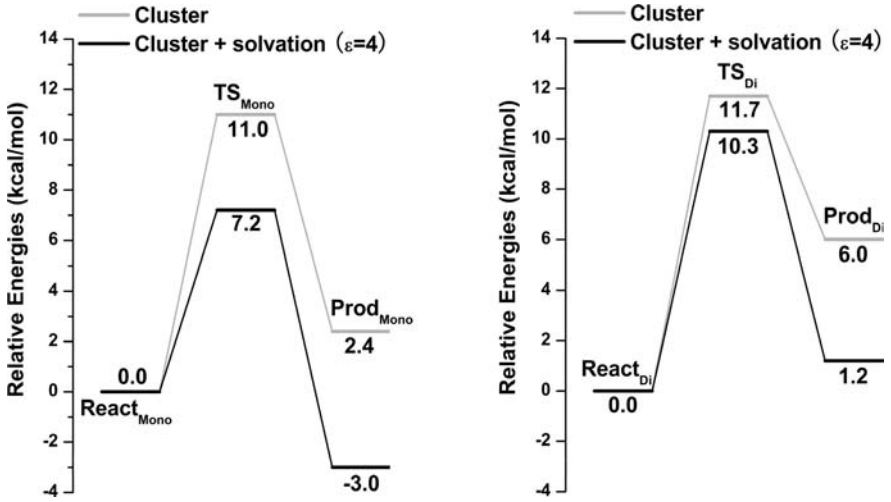

Figure 4. Calculated potential energy profiles for hydrolysis of phosphomonoester (left) and phosphodiester (right) substrates.

The O_A-P-O_L (A and L representing the attacking and leaving oxygens, respectively) angle is 162° and 171° for $React_{Mono}$ and $React_{Di}$, respectively. In $React_{Mono}$, the $P-O_A$ and $P-O_L$ distances are 3.01 and 1.70 Å, respectively, and in $React_{Di}$, the distances are 2.90 and 1.64 Å, respectively.

IV.A. Phosphomonoester Hydrolysis. From $React_{Mono}$, the transition state for the nucleophilic attack (TS_{Mono}) has been optimized and is also shown in Figure 2. We find that the hydroxide can perform the nucleophilic attack directly from its bridging position, similarly to the previously studied dinuclear zinc enzymes, phosphotriesterase (PTE),[8a] aminopeptidase from *Aeromonas proteolytica* (AAP),[8b] dihydroorotase (DHO),[8c] glyoxalase II (GlxII),[8d] acylhomoserine lactone hydrolase (AHL lactonase),[8e] RNase Z,[8f] and human renal dipeptidase (hrDP).[8g] Our previous calculations on the related trinuclear zinc enzyme PLC_{BC} also confirmed a nucleophilic attack by the hydroxide bridging Zn1−Zn3.[8h] The hydroxide proton transfers from O_A to Asp45 at TS_{Mono}, with an O_A-H distance of 1.02 Å. Thus, Asp45 acts as a general base to accept a proton from the bridging hydroxide, in a similar fashion as the aspartate residues in PLC_{BC} (Asp55)[8h] and RNase Z (Asp67).[8f] Very importantly, it is found that the $P-O_L$ bond cleavage and the nucleophilic attack occur in one concerted step. No penta-coordinated intermediate could be located, similarly to the cases of RNase Z,[8f] PLC_{BC},[8h] and endonuclease IV.[5] The barrier is calculated to be 7.2 kcal/mol (11.0 kcal/mol without inclusion of solvation effects). At TS_{Mono}, the nascent $P-O_A$ bond is 1.86 Å and the scissile $P-O_L$ bond is 2.27 Å. O_A, P, and O_L are almost in a straight line, with an angle of 167°.

It can be seen that all three zinc ions provide electrostatic stabilization to the penta-coordinated transition state. In particular, Zn2 stabilizes the leaving oxygen anion, which means that it can dissociate without protonation. There is thus no need of an additional water molecule to protonate the leaving group as in the case of PLC_{BC}.[8h] In addition, Arg48 forms stronger hydrogen bonds with the two phosphate oxygens (O_B and O_D) in TS_{Mono} compared to the reactant structure ($React_{Mono}$). This indicates that this residue also assists in lowering the barrier for hydrolysis.

Downhill from TS_{Mono}, the product complex ($Prod_{Mono}$) is formed, in which the leaving alkoxide is bound to Zn2. The overall hydrolysis reaction is calculated to be exothermic by 3.0 kcal/mol (endothermic by 2.4 kcal/mol without solvation). The reaction results in an inversion of the configuration at the phosphorus center. Since this is what has been observed experimentally too, it is possible that the product is released at this stage.

IV.B. Phosphodiester Hydrolysis. Similarly to the hydrolysis of the phosphate monoester substrate, we optimized the stationary points for the phosphodiester hydrolysis. The reaction is also here seen to proceed through a concerted transition state (TS_{Di}, Figure 3). The barrier is calculated to be 10.3 kcal/mol (11.7 kcal/mol without solvation correction), which is somewhat higher than that for phosphomonoester hydrolysis. One reason for this could be the electrostatic stabilization caused by the Arg48 residue, which is somewhat larger for the doubly anionic monoester substrate. A similar proposal has been put forward for alkaline phosphatase, which utilizes two zinc ions and a strategically located arginine residue for phosphate substrate binding, with a preference for phosphomonoesters.[21] The critical geometric parameters are slightly different from those in TS_{Mono}. For example, the $P-O_A$ and $P-O_L$ distances are 1.77 and 1.94 Å, respectively, which are shorter than those in TS_{Mono} (1.86 and 2.27 Å, respectively). In addition, the bridging hydroxide proton that is transferring to Asp67 is now much closer to that group, with O_A-H and $O_{Asp67}-H$ distances of 1.27 and 1.18 Å, respectively. The attack results in the departure of the alkoxide to form the product complex ($Prod_{Di}$). The reaction is calculated to be endothermic by 1.2 kcal/mol (6.0 kcal/mol without solvation).

It is interesting to note here that the solvation effects for the diester substrate are smaller than the corresponding ones for the monoester substrate. In particular, the barrier for the former is lowered by 1.4 kcal/mol, compared to a lowering of 3.8 for the latter. One reason is that at TS_{Mono}, more negative charge is accumulated at O_B, and the solvation effect will be larger since it is exposed at

(21) O'Brien, P. J.; Herschlag, D. *Biochemistry* **2001**, *40*, 5691–5699.

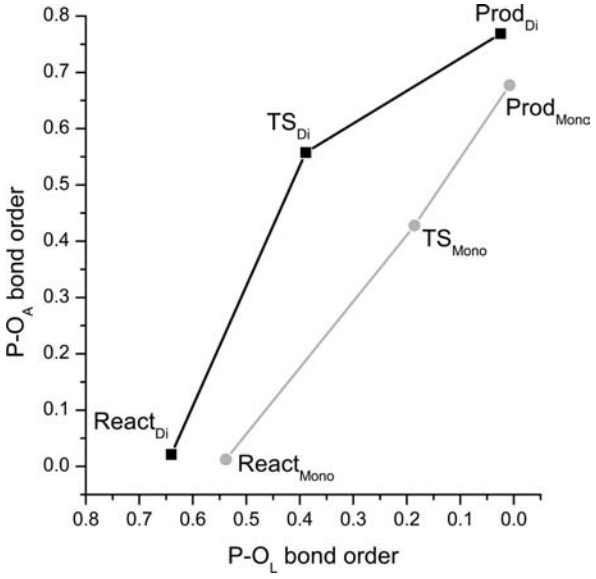

Figure 5. More O'Ferrall−Jencks plot for phosphomonoester and phosphodiester hydrolysis by nuclease P1.

the periphery of the model with only the Arg48 providing hydrogen bonding to it. For the diester substrate, O_B is methylated and does not suffer from this effect at TS_{Di}.

The calculated energies for both phosphomonoester and phosphodiester hydrolysis are shown in Figure 4. The experimental rate constant for RNA hydrolysis by nuclease P1 has been measured to be in the range of 200−900 s^{-1},[22] which can be converted to barriers of around 13−14 kcal/mol using classical transition state theory. The calculated barrier of 10.3 kcal/mol for phosphodiester hydrolysis is thus in good agreement with the experimental estimates.

From a More O'Ferrall−Jencks analysis[23] of the reactions (Figure 5), it is seen that the concerted transition state in the case of the phosphate monoester hydrolysis is quite synchronous, while in the case of the diester hydrolysis, it has a more associative character.

V. Conclusions

We have in the present paper used density functional calculations to investigate the hydrolysis reaction at the nuclease P1 active site. Both phosphate mono- and diester substrates were considered. The calculations establish that, for both substrates, the hydroxide bridging Zn1 and Zn3 performs an in-line nucleophilic attack on the phosphate group, concertedly with the dissociation of the leaving alkoxide. With the electrostatic assistance of Zn2, the leaving group can dissociate without the need of protonation, as is the case in some other enzymes. At the same transition state, Asp45 acts as a base, abstracting a proton from the nucleophilic hydroxide. Along with the three zinc ions, second-shell Arg48 is shown to provide electrostatic stabilization that lowers the barrier. The calculated barriers are in good agreement with available experimental rates.

Acknowledgment. F.H. gratefully acknowledges financial support from The Swedish Research Council (VR) and The Carl Trygger Foundation. This work was also supported by grants from the National Natural Science Foundation of China (Grant Nos. 20733002 and 20873008).

Supporting Information Available: MFJ plot with the P−O bond distances as axes. Cartesian coordinates for all structures. This material is available free of charge via the Internet at http://pubs.acs.org.

(22) Gangadhara, B. N.; Kumar, P. R.; Prakash, V. *Enzyme Microb. Technol.* **2008**, *43*, 336–342.

(23) (a) More O'Ferrall, R. A. *J. Chem. Soc. B* **1970**, 274–277. (b) Jencks, W. P. *Chem. Rev.* **1985**, *85*, 511–527.